# Influence of Sulfur and Welding Conditions on Penetration in Thin Strip Stainless Steel

*Experiments on 304 stainless steel indicate a change in temperature coefficient of surface tension from negative to positive values with sulfur contents above 50 ppm*

BY P. R. SCHELLER, R. F. BROOKS AND K. C. MILLS

ABSTRACT. Welding trials and surface tension measurements have been carried out on 304 stainless steels with sulfur (S) contents between 20 and 100 ppm. Surface tension measurements, determined by the levitated drop method, indicated that the temperature coefficient of surface tension ($d\gamma/dT$) changed from negative to positive values at S contents exceeding approximately 50 ppm. Strips with a thickness of approximately 1 mm were GTA welded on both single-electrode, small-scale and multi-electrode industrial-scale units. Welding speeds of 1 to 2 m $min^{-1}$ were used on the small-scale unit and up to 5 m $min^{-1}$ on the industrial unit. The weld penetration was found to increase, for both full and partial penetration welds, with 1) increasing sulfur contents; and 2) increasing linear energy (*i.e.*, current x voltage/welding speed). On the small scale-unit markedly higher penetration was observed in heats with S contents > 60 ppm. But the influence of S contents was only of minor importance for welds obtained on the industrial unit. It was found that the similar weld geometry could be obtained for both low (≤ 60 ppm) and high (> 60 ppm) sulfur contents by careful adjustment of welding parameters. The observed changes in weld geometry are consistent with the proposition that the fluid flow in the weld pool is dominated by thermocapillary (Marangoni) forces during the GTA welding of thin strips.

*P. R. SCHELLER is with Krupp Stahl AG, Bochum, Germany. R. F. BROOKS and K. C. MILLS are with Division of Materials Metrology, National Physical Laboratory, Teddington, Middlesex U.K.*

## Introduction

Tubes with wall thicknesses of less than 3 mm (0.12 in.) are widely used in the chemical and nuclear industries for the construction of reactors, heat exchangers, etc. In these applications it is essential that any welded joints be of high quality with regard to mechanical strength, ductility and corrosion resistance. Usually, the production of austenitic steel tubes is carried out in two steps: 1) the continuous forming of strip into tubes by rolls; and then 2) GTA welding of the seam in the tube. In order to obtain both high productivity and low production costs, it is customary to aim for high welding speeds. At the same time, it is necessary to ensure that the full penetration welds are of high quality and integrity. The capacity of the welding plant is determined by the welding speed but this and other welding parameters must be adjusted to account for differences in both the material and the geometry of the tubes.

**KEY WORDS**

304 Stainless Steel
Sulfur Content
Weld Penetration
Linear Energy
Welding Parameters
SurfaceTension
Temperature Coeff.
Thin-Strip SS
GTAW
Weld Geometry

The weld penetration is determined by the chemical composition of the weld metal and by the welding conditions since these parameters control the fluid flow patterns and subsequently, the geometry of the weld bead. Consequently, failure to optimize the welding conditions can cause a reduction in welding capacity. Additional problems may be caused by the slag precipitation on the weld surface, but this behavior was not studied in the present investigation.

In autogenous GTA welding of steel it is essential to obtain good weld penetration. However, recent investigations (Ref. 1) have shown that apparently small changes in S content of the metal can result in appreciable variations in weld penetration. Heiple and Roper (Ref. 1) proposed that variable weld penetration resulted from the following:

1) Changes in the direction and magnitude of the fluid flow in the weld pool.

2) These changes in fluid flow were controlled by the thermocapillary (Marangoni) flow arising from temperature (and consequently surface tension) gradients over the surface of the weld pool.

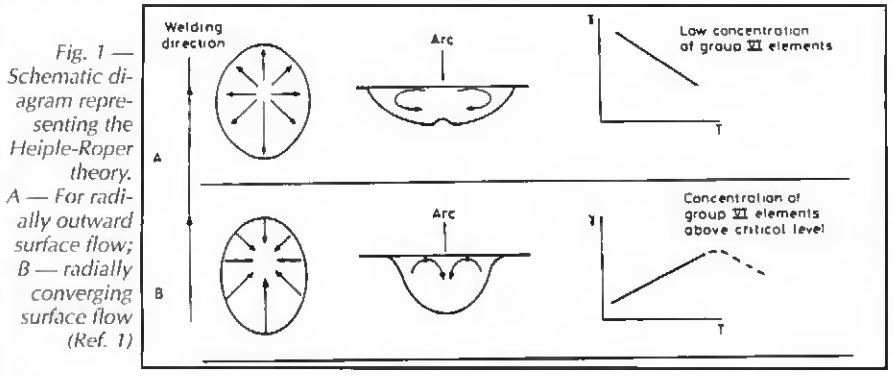


*Fig. 1 — Schematic diagram representing the Heiple-Roper theory. A — For radially outward surface flow; B — radially converging surface flow (Ref. 1)*

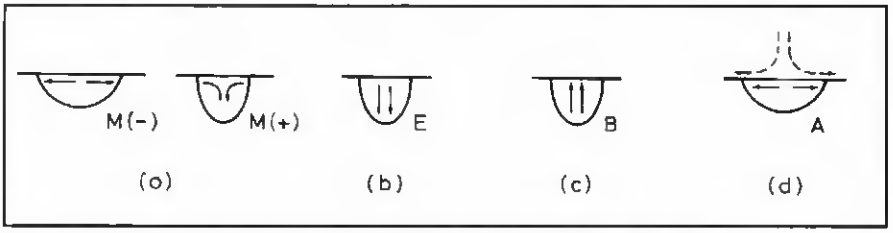


*Fig. 2 — Schematic representations of various forces on the motion of the liquid in the weld pool. A — Thermocapillary (Marangoni) forces; B — electromagnetic (Lorentz) forces; C — buoyancy; D — aerodynamic drag forces (Ref. 2).*

3) The surface flows triggering off circulatory flows within the weld pool — Fig. 1.

4) The fact that the controlling factor was the temperature coefficient of the surface tension ($d\gamma/dT$) which, in turn, was dependent upon the concentration of surface active species (such as O and S) in fusion zone.

When the soluble O or S (denoted $\underline{O}$ or $\underline{S}$) concentration is below a certain critical concentration (Fig. 1A), the surface tension is highest at the edges of the pool, and the thermocapillary flow occurs in a radially outward direction from low to high surface tension and results in melt-back at the edge of the pool, and hence, a shallow weld. However, for $\underline{O}$ and $\underline{S}$ concentrations above the critical value (approximately 50 ppm) surface flow is reversed (*i.e.*, radially inward, Fig. 1B), and hot liquid is swept to the bottom of the pool where melt-back produces a deeper weld. Implicit in this theory is the proposition that weld penetration is controlled by the fluid flow in the weld pool and not by the thermal conduction in the workpiece (Ref. 2).

In practice there are factors other than thermocapillary forces affecting the fluid flow *viz.* Lorentz (electromagnetic), buoyancy and aerodynamic drag forces, which are determined by welding conditions. The effect of these and thermocapillary forces on the fluid flow are summarized in Fig. 2. The situation is further complicated by the front-to-back motion resulting from the motion of the torch relative to the workpiece.

Welding trials (Refs. 3–5) have shown that better penetration was obtained with heats containing high sulfur contents. However, Lambert (Ref. 3) pointed out that penetration was not solely determined by S content and proposed that the concentration of heat at the center of the weld pool was also an important factor. Pollard (Ref. 4) produced partial penetration welds on both laboratory and production heats of 304 steel strips (0.7 to 2.7 mm). It was found that increasing S content had no apparent effect on laboratory heats (O, 150–200 ppm, Al <40 ppm) but did improve penetration in production heats (O, 40–80 ppm, Al <40 ppm). These results are not surprising since there would be a strong radially-inward flow in the high-O, laboratory heats regardless of S contents, but this would not be the case for the lower O production heats. Marya and Olson (Ref. 5) found that although weld penetration was higher in heats with higher S content there was no correlation between weld morphology and S content for steels containing elements such as Al and Ca. It should be noted that it is the soluble $\underline{S}$ not the total S content that affects the surface tension and $d\gamma/dT$. It has been pointed out (Ref. 2) that Al in steels will normally hold the soluble $\underline{O}$ levels to about 5 ppm but the soluble $\underline{S}$ content is not affected unless the steel contains Ca, Mg or Ce. It has been recommended (Ref. 6) that the soluble $\underline{S}$ should be >60 ppm to ensure good weld penetration (Equation 1).

$$\underline{S}(ppm) = S_{total} - 1.3\,Mg - 0.8\,Ca - 0.22\,(Ca+Ce) \quad (1)$$

A recent study (Ref. 7) has shown that although the Heiple-Roper theory applies for thick-plate (*i.e.*, penetration increases with ($d\gamma/dT$)) there are departures from a linear relationship with sheet (<3 mm). This behavior was attributed to deviations from three-dimensional heat conduction and to possible increases in the relative importance of Lorentz forces.

Consequently, the objectives of this investigation were as follows:

1) Determine the effects of sulfur content on the weld penetration in thin-sheet (approximately 1-mm-thick) 18 Cr 10 Ni stainless steels.

2) Compare the results of trials using small-scale units with those obtained in industrial practice.

3) Determine the surface tension on samples from industrial production with different S contents.

4) Determine whether the Heiple-

**Table 1 — Chemical Composition of Steel-Strip Used in this Investigation**

| Steel Type | No. | Heat No. | Strip Thickness mm | Composition, Mass % C | Si | Mn | Cr | Mo | Ni | Al | Ti | Composition, Mass ppm[a] Ca | N | $O_{tot}$ | S | P |
|---|---|---|---|---|---|---|---|---|---|---|---|---|---|---|---|---|
| 304 | 1 | 844 678 | 1.15 | .035 | 0.58 | 1.05 | 18.21 | 0.36 | 9.02 | <0.003 | 0.011 | <10 | 340 | 50–70 | 20 | 260 |
| 304 | 2 | 844 512 | 0.97 | .038 | 0.58 | 1.06 | 18.35 | 0.19 | 9.04 | <0.003 | 0.010 | <10 | 360 | 50–70 | 30 | 210 |
| 304 | 3 | 861 918/1 | 0.94 | .036 | 0.59 | 1.12 | 18.19 | 0.22 | 9.18 | <0.003 | 0.011 | <10 | 300 | 50–70 | 100 | 240 |
| 304 | 4 | 861 914/1 | 1.15 | .035 | 0.53 | 1.07 | 18.18 | 0.19 | 8.67 | <0.003 | 0.014 | <10 | 330 | 50–70 | 60 | 210 |
| 304 | 5 | 861 914/2 | 1.10 | .035 | 0.53 | 1.07 | 18.18 | 0.19 | 8.67 | <0.003 | 0.014 | <10 | 330 | 50–70 | 40 | 210 |
| 304 | 6 | 861 918/2 | 0.95 | .036 | 0.59 | 1.12 | 18.19 | 0.22 | 9.18 | <0.003 | 0.011 | <10 | 300 | 50–70 | 70 | 240 |

(a) Accuracy of chemical analysis = ±5 ppm.

Roper theory is applicable for thin plate.

## Experimental

### Materials

The steels were 80-ton AOD (argon-oxygen decarburization) heats of 18 Cr, 10 Ni, 304 type stainless steels rolled to approximately 1 mm (0.04) thickness. Details including chemical composition and strip thickness are given in Table 1. The S contents of these steels were varied between 20 and 100 ppm, all other elements were kept reasonably constant.

### Surface Tension Measurement

The surface tensions of the steels were measured using the levitated drop method (Ref. 8). In this technique, a sample of known mass (m) is levitated in an electromagnetic coil and the natural oscillation frequency (w) is monitored continuously. The surface tension can be calculated from the Rayleigh formula given in Equation 2.

$$\gamma = 3\,\pi\,m\,\omega^2/8 \qquad (2)$$

A sample (approximately 0.4 g) was levitated in an electromagnetic coil, which was connected to a 15 kW, Radyne RF generator operating at 450 Hz. The frequency of the natural oscillation was determined by projecting the image of the molten, oscillating drop onto a photodetector and analyzing the frequency spectrum by means of a Wavetek waveform analyzer. The temperature of the drop was measured by a two-color pyrometer.

The sample was prevented from oxidation by maintaining a continuous flow of purified gas (Ar, He and $H_2$) flowing through a silica tube that ran through the interior of the coil. The temperature of the drop was adjusted by altering either the ratio of these gases or the power supplied to the coil.

It has been found in practice that a frequency spectrum containing 3 or 5 peaks is obtained and not the single (Rayleigh) frequency ($\omega_R$) predicted by Equation 2. The splitting is due to the effect of electromagnetic pressure, which results in an apparent increase in surface tension. The results obtained in this study were derived from Equation 2, using the central frequency of the spectrum as the Rayleigh frequency. However, recently an expression has been proposed (Ref. 9) for separating the effect of electromagnetic pressure from the surface tension; the true surface tension being derived by Equation 3 where the subscripts 1 to 5 represent the various peaks and $\omega_T$ the transitional frequency at about 5 Hz.

**Table 2 — Welding Conditions Used in Trials and Results of Welding Penetration or Full Penetration**

| | | | Weld Bead Shape | | | | | | | |
|---|---|---|---|---|---|---|---|---|---|---|
| No | S-Content mass % (ppm) | Strip Thickness mm | Front Width $W_f$ mm | Back Width $W_b$ mm | Depth d mm | $d/W_f$ | $W_b/W_f$ | Welding Speed $S_w$ mm/s | Current I Amp | Linear Energy[a] E $Jmm^{-1}$ |
| 1-1 | | | 3.10 | 1.05 | | | 0.33 | 16.7 | 100 | 90 |
| 2 | | | 2.15 | — | 0.72 | 0.33 | | 25 | 100 | 60 |
| 3 | | | 1.90 | — | 0.52 | 0.27 | | 33.3 | 100 | 45 |
| 4 | 0.002 | 1.15 | 4.08 | 2.67 | | | 0.65 | 16.7 | 150 | 135 |
| 5 | (20) | | 2.88 | 0.72 | | | 0.25 | 25 | 150 | 90 |
| 6 | | | 2.44 | — | 0.80 | 0.33 | | 33.3 | 150 | 68 |
| 7 | | | 5.32 | 4.51 | | | 0.85 | 16.7 | 200 | 180 |
| 8 | | | 3.59 | 1.73 | | | 0.50 | 25 | 200 | 120 |
| 9 | | | 2.70 | — | 0.95 | 0.35 | — | 33.3 | 200 | 90 |
| 2-1 | | | 3.23 | 2.20 | | | 0.68 | 16.7 | 100 | 90 |
| 2 | | | 2.06 | — | 0.97 | 0.47 | | 25 | 100 | 60 |
| 3 | | | 1.95 | — | 0.68 | 0.35 | | 33.3 | 100 | 45 |
| 4 | 0.003 | 0.97 | 4.32 | 3.82 | | | 0.88 | 16.7 | 150 | 135 |
| 5 | (30) | | 2.94 | 2.05 | | | 0.70 | 25 | 150 | 90 |
| 6 | | | 2.70 | 0.76 | | | 0.28 | 33.3 | 150 | 68 |
| 7 | | | 4.61 | 4.56 | | | 0.99 | 16.7 | 200 | 153 |
| 8 | | | 3.59 | 3.38 | | | 0.94 | 25 | 200 | 120 |
| 9 | | | 3.15 | 1.76 | | | 0.54 | 33.3 | 200 | 90 |
| 3-1 | | | 3.03 | 2.50 | | | 0.83 | 16.7 | 100 | 90 |
| 2 | | | 2.26 | 1.20 | | | 0.53 | 25 | 100 | 60 |
| 3 | | | 1.82 | — | 0.94 | 0.52 | | 33.3 | 100 | 45 |
| 4 | 0.010 | 0.94 | 4.02 | 3.97 | | | 0.99 | 16.7 | 150 | 135 |
| 5 | (100) | | 3.17 | 1.97 | | | 0.62 | 25 | 150 | 90 |
| 6 | | | 2.61 | 1.26 | | | 0.48 | 33.3 | 150 | 68 |
| 7 | | | 5.73 | 5.46 | | | 0.95 | 16.7 | 200 | 180 |
| 8 | | | 3.91 | 3.61 | | | 0.92 | 25 | 200 | 120 |
| 9 | | | 2.96 | 2.79 | | | 0.94 | 33.3 | 200 | 90 |
| 4-1 | | | 2.50 | 1.15 | — | | 0.45 | 16.7 | 100 | 90 |
| 2 | | | 1.81 | — | 0.75 | 0.41 | | 25 | 100 | 60 |
| 3 | | | 1.58 | — | 0.58 | 0.37 | | 33.3 | 100 | 45 |
| 4 | 0.006 | 1.15 | 3.65 | 2.45 | — | | 0.67 | 16.7 | 150 | 135 |
| 5 | (60) | | 2.73 | 0.50 | — | | 0.18 | 25 | 150 | 90 |
| 6 | | | 2.13 | — | 0.72 | 0.34 | | 33.3 | 150 | 68 |
| 7 | | | 7.33 | 7.04 | — | | 0.96 | 16.7 | 200 | 180 |
| 8 | | | 3.34 | 1.67 | — | | 0.50 | 25 | 200 | 120 |
| 9 | | | 2.90 | 1.01 | — | | 0.35 | 33.3 | 200 | 90 |
| 5-1 | | | 2.77 | 0.41 | — | | 0.15 | 16.7 | 100 | 90 |
| 2 | | | 1.86 | — | 0.68 | 0.37 | | 25 | 100 | 60 |
| 3 | | | 1.75 | — | 0.51 | 0.29 | | 33.3 | 100 | 45 |
| 4 | 0.004 | 1.13 | 4.01 | 2.83 | — | | 0.71 | 16.7 | 150 | 135 |
| 5 | (40) | | 2.74 | — | 1.04 | 0.38 | | 25 | 150 | 90 |
| 6 | | | 2.34 | — | 0.76 | 0.32 | | 33.3 | 150 | 68 |
| 7 | | | 7.57 | 7.01 | — | | 0.94 | 16.7 | 200 | 153 |
| 8 | | | 4.07 | 2.54 | — | | 0.62 | 25 | 200 | 120 |
| 9 | | | 3.25 | 1.41 | — | | 0.43 | 33.3 | 200 | 90 |
| 6-1 | | | 3.35 | 2.67 | — | | 0.80 | 16.7 | 100 | 90 |
| 2 | | | 1.87 | 0.63 | — | | 0.34 | 25 | 100 | 60 |
| 3 | | | 1.57 | — | 0.60 | 0.38 | | 33.3 | 100 | 45 |
| 4 | 0.007 | 0.95 | 4.36 | 4.22 | — | | 0.97 | 16.7 | 150 | 135 |
| 5 | (70) | | 2.73 | 1.84 | — | | 0.67 | 25 | 150 | 90 |
| 6 | | | 2.20 | 0.89 | — | | 0.40 | 33.3 | 150 | 68 |
| 7 | | | 7.18 | 6.98 | — | | 0.97 | 16.7 | 200 | 180 |
| 8 | | | 4.28 | 3.92 | — | | 0.93 | 25 | 200 | 120 |
| 9 | | | 3.21 | 2.46 | — | | 0.77 | 33.3 | 200 | 90 |

(a) Linear energy E is defined as [current (I)×voltage (u)/welding speed ($S_w$)]
Other welding parameters: Voltage = 15 V; Arc Length = 0.5 mm; Electrode W 2% $ThO_2$, diam 2.4 mm, tip angle = 60-deg. Torch gas: Ar + 2% $H_2$: Flow Rates, front 10 L $min^{-1}$, back 16 L $min^{-1}$, ceramic torch nozzle 10-mm diam.

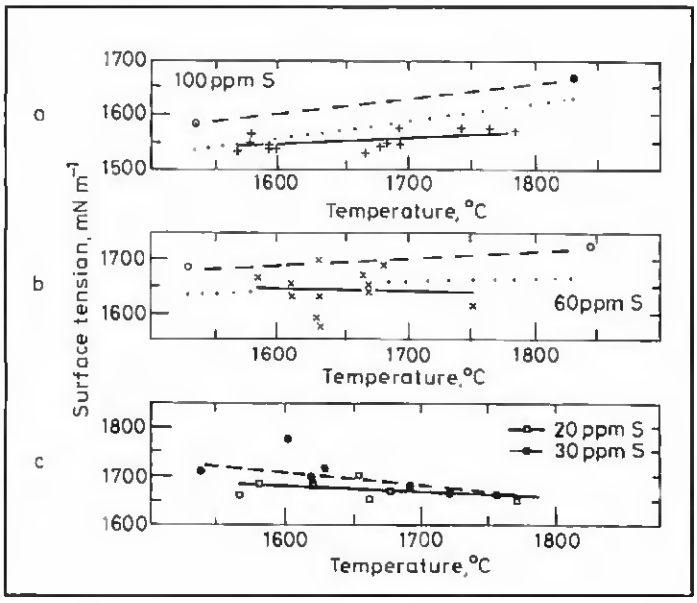


*Fig. 3 — Surface tensions of 18 Cr 8 Ni 304-type stainless steels with: A — 100 ppm S; B — 60 ppm S; C — 20–30 ppm S; –x, this investigation, --, calculated values (Ref. 10);—, calculated values (Ref. 10) using corrected values for surface tension.*

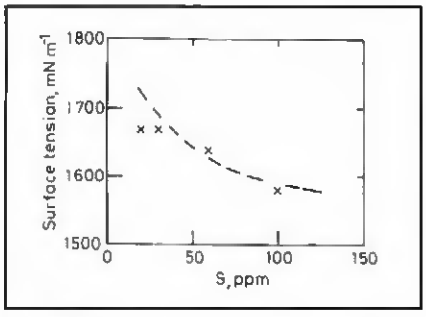


*Fig. 4 — Surface tensions of 18 Cr 8 Ni 304-type steels at 1800°C as a function of S content; - -, curve based on data for other 18 Cr 8 Ni stainless steels; x, this investigation.*

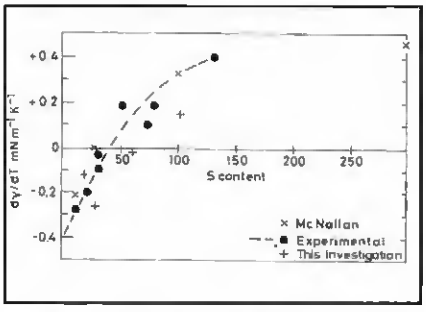


*Fig. 5 — Temperature coefficients of surface tension (dγ/dT) of 18 Cr 8 Ni stainless steels for the temperature interval (1550–1800°C) as a function of total S content.*

$$\bar{\omega}_R^2 = \frac{1}{5}\sum\left(\begin{matrix}\omega_1^2+\omega_2^2+\omega_3^2+\\ \omega_4^2+\omega_5^2\end{matrix}\right) - \omega_1^2\left[1.9+1.2\left(\frac{g}{2a\omega_1^2}\right)^2\right] \quad (3)$$

Typically the application of this expression results in a decrease of 2 to 3% to the surface tensions derived from the central frequency; consequently, the surface tension results were subjected to a correction of –2.5%.

#### Welding Trials

Full penetration, bead-on-plate welds were carried out on strips from 304 stainless steel using a single electrode, small-scale unit using linear energies of 40 to 180 J $mm^{-1}$. Details of welding conditions are given in Table 2.

The strip samples had dimensions of 1200 x 100 x 1 mm (48 x 4 x 0.04 in.) and were held in rigid, brass fixtures. The strips were cleaned before welding. The welding was always carried out in the same direction and the length of the weld run was about 1000 mm (40 in.). Penetration was measured by sectioning the weld run at a position about 450 mm from the start to ensure that all welding parameters were uniform. Since the weld surface was very regular, only one section per weld was taken. Although the (depth/width), *i.e.*, (D/W) partial penetration, welds provide a more reliable measure of weld penetration, it is more customary to carry out full-penetration welds on thin plate and thus the ratio of (back-to-front) widths ($W_b/W_f$) has been primarily used in this study.

Penetration was determined by measuring the widths of the front and back welds for full-penetration welds and by etching sections of the weld with 1:1 $HNO_3$ and measuring the depth/width (D/W) ratio of partial penetration welds in an optical microscope.

Welding trials were also carried out with high-efficiency industrial units with 1 to 3 electrodes. Strips of the same heat were formed into tubes and welded at speeds of up to 5 m $min^{-1}$. The effect of welding conditions on penetration for these industrial trials was not investigated in detail, but the weld pool profiles obtained were compared with those obtained in investigations using small scale units.

## Results and Discussion

#### Surface Tension

Surface tensions were obtained for all the steels. Typical results for surface tension as a function of temperature are shown in Fig. 3 for steels with S contents smaller and greater than the critical composition where dγ/dT = 0. The surface tensions at 1800°C (3272°F) of all steels[1] are shown as a function of total S content in Fig. 4, and it can be seen that surface tension decreases markedly with S content. It can also be seen that the dependence of surface tensions of 18 Cr 8 Ni austenitic steels upon S content, derived by McNallan and Dehroy (Ref. 10) from thermodynamic calculations, are in excellent agreement with the experimental values when allowance is made for the fact that the calculated values are based on surface tension data (Refs. 11, 12), which were not corrected for the transitional frequency term in Equation 3.

There are insufficient number of experimental points in Fig. 3 to derive accurate values of the temperature coefficient dγ/dT, which can only be derived with >20 measurements of surface tension. However, accurate values of dγ/dT have been obtained in our laboratory for other heats of 18 Cr 8 Ni 304 and 316 type austenitic stainless steels and these are shown as a function of S content in Fig. 5. It can be seen that the values of dγ/dT for the temperature range 1550° –1800°C calculated by McNallan and Debroy (Ref. 10) are in excellent agreement with the values recorded experimentally, especially when probable uncertainties for S analyses (±5 ppm) are taken into account. It should be noted that dγ/dT is a function of both S content and temperature and the calculated values cited in Fig. 5 refer to a mean temperature of 1680°C (3056°F). It can be seen from Fig. 5 that the crossover point where (dγ/dT) = 0 occurs at about 40 to 50 ppm S. This is consistent with the results of welding trials on thick plate, which suggest that good penetration is associated with S >50 ppm (Refs. 1, 6).

#### Welding Trials

The micrographs showing the full penetration welds obtained when welding steels 1 and 3 (with 20 and 100 ppm S, respectively) under identical condi-

tions are shown in Fig. 6. It can be seen that better weld penetration is obtained for the steel with high S content.

The ratio ($W_b/W_f$) for full-penetration welds was also found to increase with increasing S content when welding with constant linear energies of 90 J mm$^{-1}$ — Fig. 7. The improvement in the $W_b/W_f$ ratio was clearly evident in heats with S contents higher than 60 ppm. Thus, the results obtained are in general agreement with previous investigations (Refs. 1, 3, 4, 13–15) in that penetration was found to be dependent upon S content and thus upon the temperature coefficients of the surface tension ($d\gamma/dT$) for the weld pool. The latter affects the velocities and direction of the surface flows, which are typically between 0.5 and 2 ms$^{-1}$ (Refs. 15, 16).

It can be seen from Fig. 8 that the $W_b/W_f$ ratio not only increases with increasing S content, but also with increasing linear energy[2]. However, the width of the weld also increases at the same time. Although there are insufficient measurements to establish a reliable dependency on linear energy, the curves shown in Fig. 8 clearly reveal the stated tendency. Results for the ratio $W_b/W_f$ for steels with S $\leq$ 60 ppm welded with constant linear energies show (Fig. 9): 1) a large amount of scatter and 2) no visible relationship with S content. The small variation in strip thickness is also contributed to the scatter in $W_b/W_f$. However, as can be seen from Fig. 9, recorded values for $W_b/W_f$ with S contents of 70 and 100 ppm are clearly higher than for those with S $\leq$ 60 ppm, especially at low linear energies. Furthermore, it is shown that $W_b/W_f$ ratios are very sensitive to minor variations in energy input.

In the welding trials, the energy input was increased to very high levels (180 J mm$^{-1}$). However, for most practical applications, reasonable weld geometries could be obtained with 120 J mm$^{-1}$ for samples with S $\leq$ 60 ppm and 90 J mm$^{-1}$ for heats with S contents between 70 to 100 ppm. The three micrographs in Fig. 10 show profiles of welds carried out on steel strips with 20, 60 and 100 ppm S. The geometry of these welds is similar. The linear energy used in these tests was 90 J mm$^{-1}$ for the 20 and 60 ppm S heats and 67.5 J mm$^{-1}$ for the 100 ppm S sample. Welds obtained using higher linear energies were found to be very wide and the cross-sections showed irregularities in depth.

Since thermocapillary forces appear to be predominant for the forces affecting the fluid flow in the weld pool, Burghardt and Heiple (Ref. 13) proposed that changes in welding parameters on weld penetration could be construed in terms of their effect on temperature gradient dT/dx across the weld pool surface. Thus, increases in dT/dx would cause decreases and increases, respectively, in penetration for low-S and high-S heats. Other investigations have been in essential agreement with this proposition, but a recent study (Ref. 7) has shown that there are deviations from the Heiple-Roper theory when dealing with thin (<3-mm) sheet. This behavior could be attributed to deviations from three-toward two-dimensional heat conduction and possibly to an increase in the relative magnitude of the Lorentz forces.

The increased penetration with increased linear energy recorded in this investigation has also been observed by Burghardt and Heiple (Ref. 13) but only for high-S heats. Their investigations were, however, carried out 1) at much higher (5X) linear energies, 2) with 20-mm (0.8-in.) thick plate, 3) with very low welding speeds (2.5 mms$^{-1}$) and 4) for partial penetration welds. The increase in $W_b/W_f$ with increasing linear energy recorded in this investigation probably reflects changes in the geometry of the circulation vortices in the weld pool. The change from partial to full penetration is probably very sensitive to the geometry of the circulation flow and could result in the departure from three-dimensional heat conduction. It is also possible that the high welding speeds used in this investigation could have affected the results by creating marked asymmetry in both the flow patterns and the weld pool shape, *i.e.*, in the direction of welding.

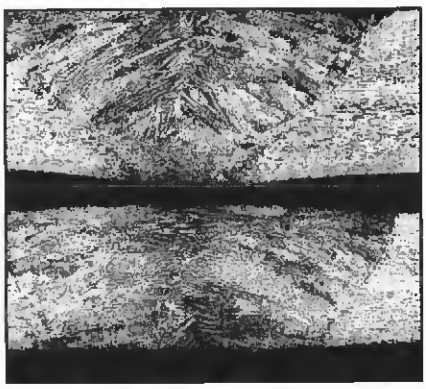

*Fig. 6 — Comparison of micrographs of welds in steels with: A — 20 ppm S; B — 100 ppm S carried out under identical welding conditions.*

Mathematical modeling of the fluid flow in the weld pool (Ref. 17) has established that it is possible to obtain deep penetration by using high currents and a sharply focused heat input even when the thermocapillary forces produce a radially outward surface flow. The strong

*1. The mean temperature of the weld pool is probably around 1800°C.*

*2. Linear energy is defined as the heat supplied per unit length of weld and is given by (current x voltage)/welding speed.*

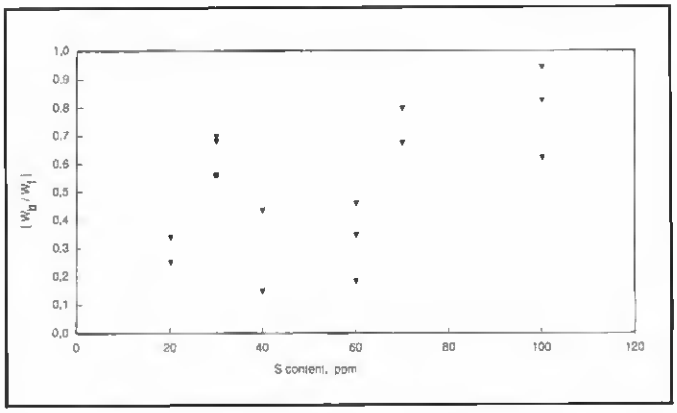


*Fig. 7 — $(W_b/W_f)$ ratio as a function of S content of the steel for constant linear energies of 90 J mm-1.*

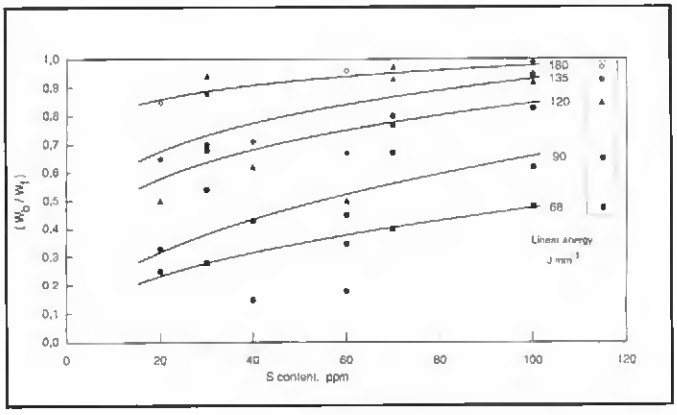


*Fig. 8 — $(W_b/W_f)$ ratio as a function of S content for different linear energies.*

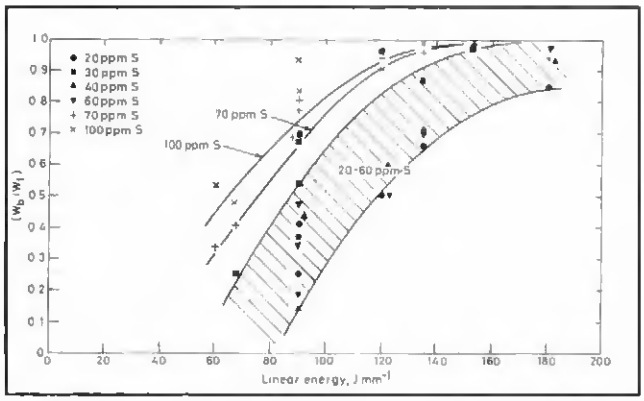


*Fig. 9 — (Wb/Wf) ratio as a function of linear energies. Curves represent welding results from small-scale unit.*

dependence of $W_b/W_f$ upon linear energy for low S heats in this investigation suggests that for the short arc length used in this study, high currents and low welding speeds appear to have a strong affect on the circulation flows. For a focused arc, the high surface velocities associated with thermocapillary flow extends to a relatively small region, according to Kou and Wang (Ref. 18). Thus, the balance between thermocapillary (Marangoni) and electromagnetic forces is sensitive and depends upon the precise nature of the welding conditions.

Another series of trials was carried out using high-speed industrial welding units. In this welding process, the weld solidifies under compressive stress and the surface is smoothed by a roll. Different welding conditions were used in the welding of tubes of the materials under investigation without adjustment for the S content of each heat. Micrographs of two butt joints are shown in Fig. 11 and indicated that $W_b/W_f$ ratios were similar despite the difference in S contents of the steels. The $W_b/W_f$ ratios for the industrial welding of approximately 1-mm-thick tubes are compared with values obtained in the small scale welding trials in Fig. 12. It can be seen that $(W_b/W_f)$ values in industrial trials were virtually constant and independent of linear energy and that any differences in the ratio due to differences in S content were small. These findings differ from those recorded for the small scale trials, the differences in behavior can be attributed to the use of one to three electrodes with various energy inputs to each one, and higher (2 to 3X) welding speeds in the industrial trials. This clearly demonstrates that in the welding of sheet it is possible to alter the penetration by changes in welding conditions.

The $W_b/W_f$ ratio is one of several parameters that are important in industrial welding. On the basis of the results obtained in this investigation, the welding speed can be increased and the weld geometry maintained constant providing the S content of the steel is greater than 60 ppm. Consequently, in order to maintain maximum throughput (*i.e.*, welding speed), the welding parameters must be adjusted to individual S contents, taking into account the concentrations of interacting elements such as Ca, Al, etc. (Equation 1). However, the S content does not affect the optimum welding condition for steel heats with S $\leq$ 60 ppm, and thus, welding parameters need not be adjusted for each heat. No cracks were detected in the welds produced with both the small scale and industrial units. This is due to the primary ferritic solidification of 304 stainless steel.

If a material with a high S content is welded without compressive stress on a one-electrode plant, an indent may occur in the middle of the joint. Furthermore, high S contents have a deleterious effect on hot and cold workability and corrosion resistance. Consequently, any gains in throughput (*i.e.*, welding speed) derived by using heats with high S contents must be balanced against the resultant losses in workability and corrosion resistance. Thus, the final selection of the composition will depend upon the final application of the tubes.

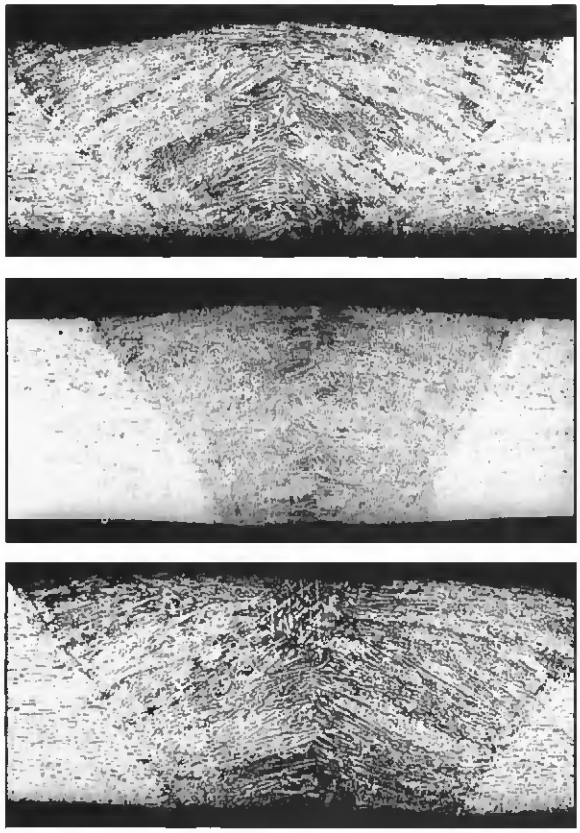

*Fig. 10 — Micrographs of butt joints on tubes from industrial welding trials. A — Pipe diameter 30 mm, wall thickness 0.98 mm, S content 30 ppm; B — Pipe diameter 40 mm, wall thickness 0.96 mm, S content 100 ppm.*

## Conclusions

It was the aim of this investigation to determine the effects that the S content of a steel has upon both the temperature coefficient of the surface tension ($d\gamma/dT$) and the weld penetration of steel strips, and also how the welding parameters influence the weld profile. The following conclusions can be drawn from the results obtained in this investigation:

1) The temperature coefficient of surface tension ($d\gamma/dT$) changes from negative to positive values when the S content exceeds 50 ppm, *i.e.*, in essential agreement with the observed changes in welding behavior.

2) The weld penetration in thin strip increases with increasing S content and increasing linear energies on small-scale units, and for heats with S $\leq$ 60 ppm, a similar weld geometry to that obtained for high S casts can be maintained for higher welding speeds by an increase in the linear energy.

3) On industrial multi-electrode plants, the geometry of the weld can be

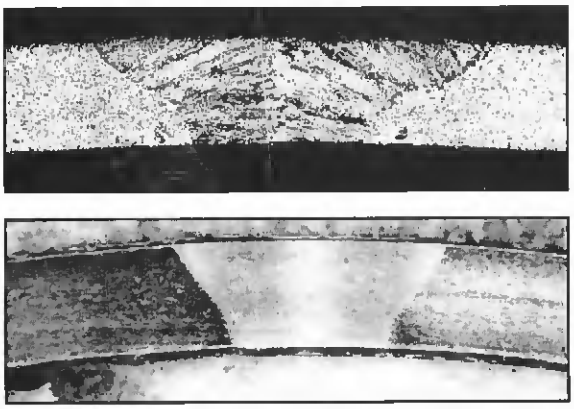

*Fig. 11 — Comparison of $W_b$ /$W_f$ ratios obtained for butt joint welds obtained on industrial units with those obtained on small-scale units denoted as curves (taken from Fig. 9); (Ref. 2) number of cathodes used.*

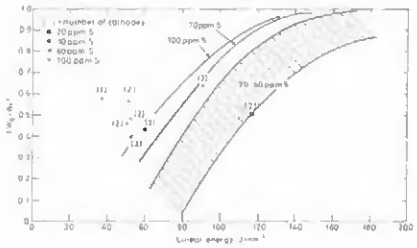

*Fig. 12 — The $W_b$ $W_f$ ratios for small scale welding trials as compared to industrial welding trials.*

influenced markedly by welding parameters. The influence of S was found to be only of minor importance in trials where the welding parameters were not tailored to the specific S contents of the casts. Higher S contents do permit higher welding speeds to be achieved, especially on one-electrode plants. However, any gains from increased throughput (*i.e.*, welding speed), must be balanced against the inferior hot and cold workability and corrosion resistance of high-S casts.

*Acknowledgment*

This work was partially financed by the European Coal and Steel Community for the period 1987–1990.

*References*

1. Heiple, C. R., and Roper, J. R. 1982. *Welding Journal* 61(4): 973.

2. Mills, K. C., and Keene, B. J. 1990. *Intl. Materials Review*, 35: 185–216.

3. Lambert, J. A. 1991. *Welding Journal*, 70(5): 41–52.

4. Pollard, B. 1988. *Welding Journal* 67(9): 202-s to 213-s.

5. Marya, S. K., and Olson, D. L. 1989. *Mem. Et. Sci Rev. Met.* (1): 25–34.

6. Lancaster, J. F., and Mills, K. C. IIW *Recommendations* 212-796-91.

7. Mills, K. C., Shirali, A., and Brooks, R. F. 1993. *Unpublished results, National Physical Laboratory.*

8. Keene, B. J., Mills, K. C., Brooks, R. F. 1985. *Mater. Sci. Technol.* 1, p. 568.

9. Cummings, D., and Blackburn, D. J. 1991. *Fluid Mech*, 224, p. 395.

10. McNallan, M. J., and Debroy, T. 1991. *Metall. Trans.* B, 22B, pp. 557, 589, 560.

11. Sahoo, P., and Debroy, T. 1987. *Metall. Trans.* 8, 18B, pp. 597–601.

12. Keene, B. J., Bryant, J. W., Mills, K. C., and Hondros, E. D. 1983. *Canad. Metall Quart.* 21, pp. 393–403.

13. Burghardt, P., and Heiple, C. R. 1986. *Welding Journal* 65(6): 150-s to 155-s.

14. Walsh, D., and Savage, W. F. 1985. *Welding Journal* 64(5): 137-s to 139-s.

15. Steffens, H. D., Thier, H., Killing, R., and Sievers, E. R., Li, Zi. 1990. *Schweissen und Schneiden*, 42(11): 571–575.

16. Heiple, C. R., Burghardt, P., Roper, J. R., Long, J. L. 1983. Proceedings: *The Effects of Residual Impurity and Microalloying Elements on Weldability and Weld Properties.* The Welding Institute, London, England.

17. Oreper, G. M., Eagar, T. W., and Szekely, J. 1983. *Welding Journal* (11): 307-s to 312-s.

18. Kou, S., and Wang, Y. H. 1986. *Welding Journal* (3): 63-s to 70-s.

CLARIFICATION: *Puckering Phenomenon and its Prevention in GMA Welding of Aluminum Alloys* by H. Miyazaki, *et al.*, pp. 277-s to 284-s, 12/94. Information that did not appear in the original printing of the article has been added to the figures below.

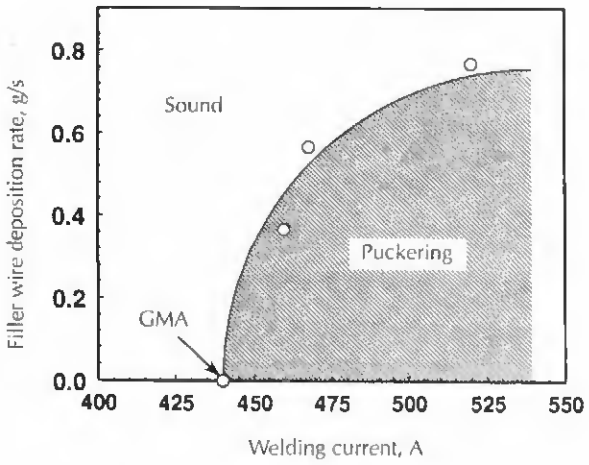


*Fig. 4 — Effect of welding current and filler metal wire addition on puckering phenomenon for bead-on-plate experiments. Welding gun angle: 20 deg.*

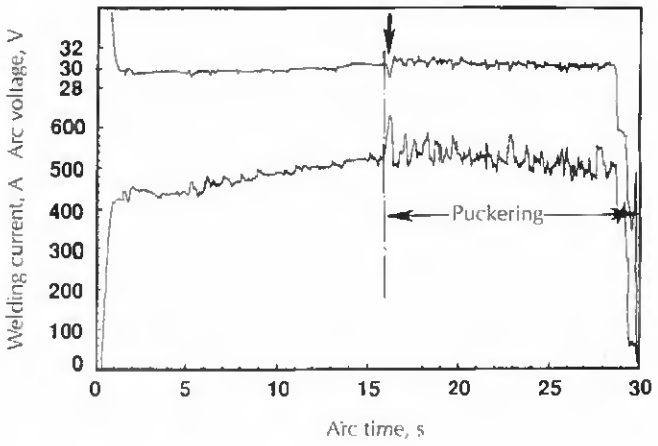


*Fig. 5 — Oscillograms of welding current and arc voltage during puckering. Filler metal wire deposition rate: 0.78 g/s.*

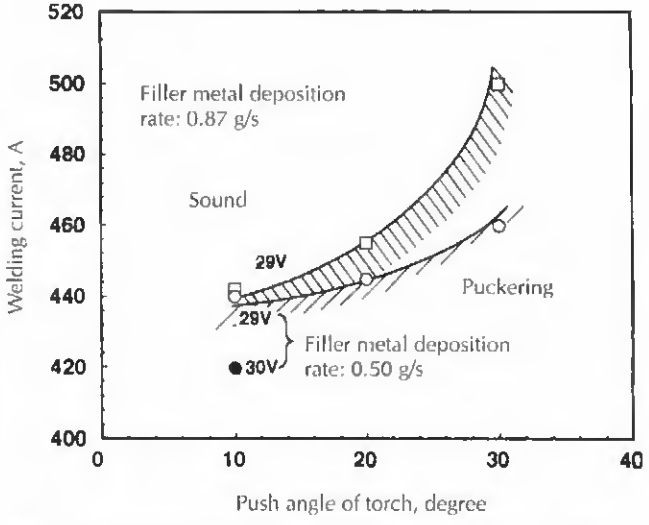


*Fig. 6 — Effect of welding gun push angle on the threshold puckering current in the DW GMA welding process. Bead-on-plate weld. Open mark: sound weld; solid mark: puckering bead.*

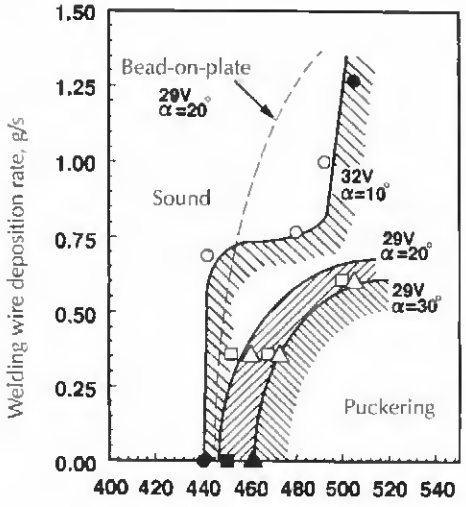


*Fig. 7 — Extending the threshold welding current with filler metal wire addition in the case of the DW GMA process. Fillet weld.*

*α: Push angle of welding gun.*

*Solid mark: Puckering bead.*

*Open mark: Sound bead.*

*Fillet weld* ——

*Bead-on-plate* - - - -

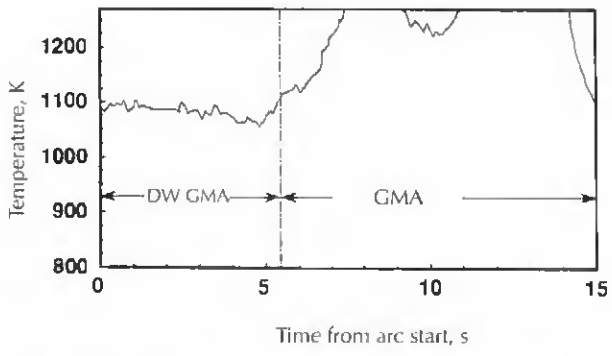


*Fig. 9 — Temperature change in the molten pool when changing the welding process from DW GMA to conventional GMA welding.*

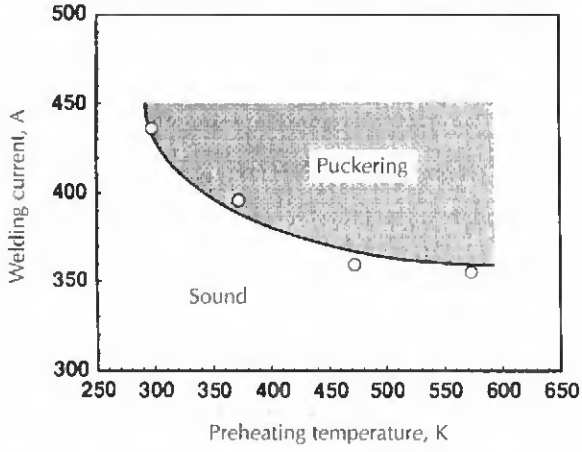


*Fig. 10 — Effect of preheating temperature of the base metal on puckering phenomenon.*